UCRL-JC-123775
PREPRINT

CONF-961005--3

Hydrodynamic Instability Experiments on the Nova Laser

B. A. Remington, S. G. Glendinning, D. H. Kalantar, K. S. Budil, O. L. Landen,
B. A. Hammel, M. M. Marinak, S. V. Weber, C. J. Keane, S. W. Haan,
A. Rubenchik, R. J. Wallace, M. H. Key, J. P. Knauer, D. Ofer, W. W. Hsing,
D. Galmiche, M. A. Blain, W. M. Wood-Vasey, D. Shvarts

This paper was prepared for submittal to the
16th IAEA International Conference on Plasma Physics
and Controlled Nuclear Fusion Research
Montreal, Canada
October 7-11, 1996

August 9, 1996

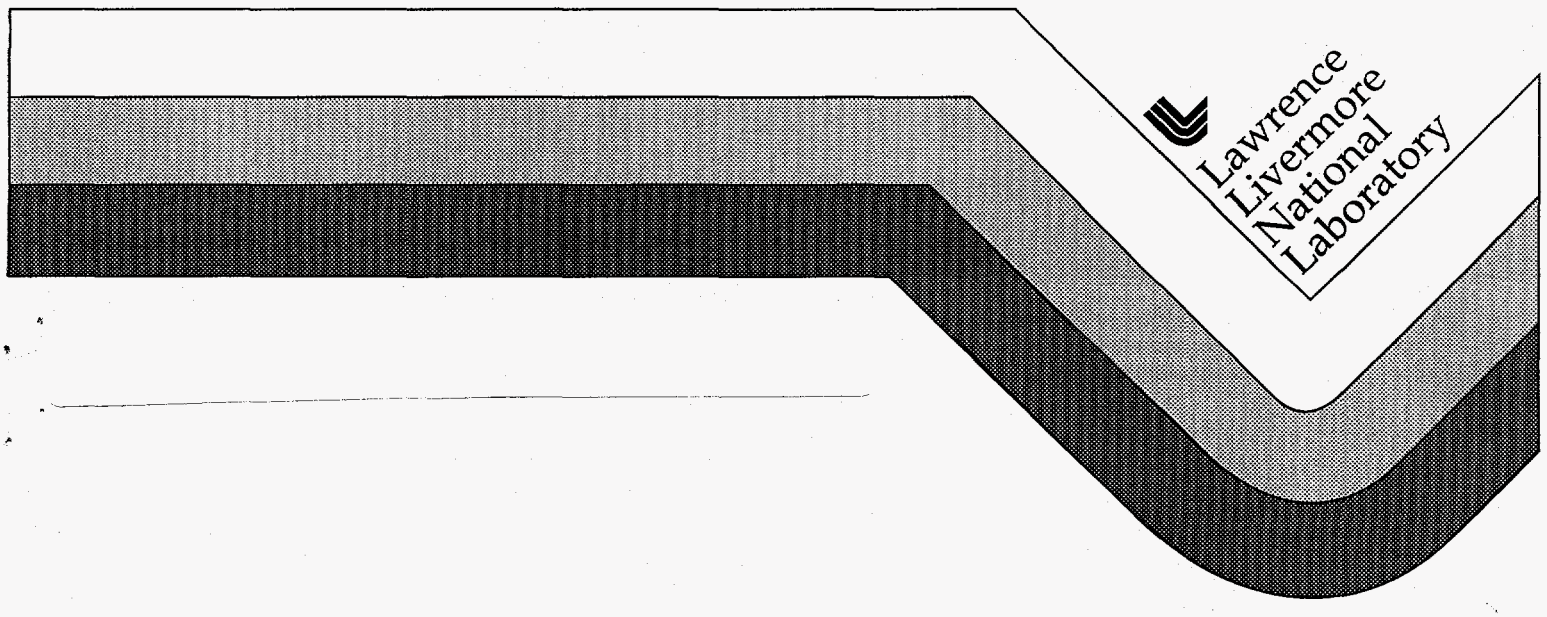

Paper for the 16th IAEA International Conference on
Plasma Physics and Controlled Nuclear Fusion Research
October 7-11, 1996, Montreal, Canada

Hydrodynamic instability experiments on the Nova laser*

B.A. Remington, S.G. Glendinning, D.H. Kalantar, K.S. Budil,
O.L. Landen, B.A. Hammel, M.M. Marinak, S.V. Weber, C.J. Keane,
S.W. Haan, A. Rubenchik, and R.J. Wallace

Lawrence Livermore National Laboratory, Livermore, CA,

M.H. Key

Rutherford-Appleton Laboratory UK, and
Lawrence Livermore National Laboratory, Livermore, CA

J.P. Knauer, D. Ofer

Laboratory for Laser Energetics, University of Rochester

W.W. Hsing

Los Alamos National Laboratory, Los Alamos, NM

D. Galmiche, M.A. Blain

CEA Centre d'Etudes de Limeil-Valenton, France

W.M. Wood-Vasey

Harvey-Mudd College, Clairmont, CA

D. Shvarts

Nuclear Research Center, Negev, Israel

August 9, 1996

Abstract

Hydrodynamic instabilities in compressible plasmas play a critical role in the fields of inertial confinement fusion (ICF), astrophysics, and high energy-density physics. We are investigating hydrodynamic instabilities such as the Rayleigh-Taylor (RT) instability, at high compression at the Nova laser in a series of experiments, both in planar and in spherical geometry. In the indirect drive approach, a thermal x-ray drive is generated by focusing the Nova laser beams into a Au cylindrical radiation cavity (hohlraum). Issues in the instability evolution that we are examining are shock propagation and foil compression, RT growth of 2D versus 3D single-mode perturbations, drive pulse shape, perturbation location at the ablation front versus at an embedded interface, and multimode perturbation growth and nonlinear saturation. The effects of convergence on RT growth are being investigated both with hemispherical implosions of packages mounted on the hohlraum wall and with spherical implosions of capsules at the center of the hohlraum. Single-mode perturbations are pre-imposed at the ablation front of these capsules as a seed for the RT growth. In our direct drive experiments, we are investigating the effect of laser imprinting and subsequent RT growth on planar foils, both at λ_{Laser}=1/3 μm and 1/2 μm. An overview is given describing recent progress in each of these areas.

I. Introduction

Hydrodynamic instabilities play a critical role in the efforts to achieve thermonuclear ignition through inertial confinement fusion (ICF). For laser-driven ICF, the design space for ignition is typically mapped out in terms of laser power versus laser energy. In these terms, the upper, high-power boundary is set by the threshold for initiating laser-plasma instabilities (SRS, SBS, filamentation, etc.). The low-power boundary is set by the limits imposed by hydrodynamic instabilities (Rayleigh-Taylor, Richtmyer-Meshkov, Kelvin-Helmholtz). For example, for a given total laser energy, if one designs an ignition capsule to implode near the low power limit, the capsule necessarily must have a higher aspect ratio ($R/\Delta R$) to still achieve the critical implosion velocity required for ignition. However, high aspect ratio designs are more prone to shell breakup, inner wall distortions, and performance degradation due to hydrodynamic instabilities. Hence, one has to balance one's confidence at being able to predict levels of hydrodynamic instabilities and their effect on the implosion against the risk of triggering parametric laser-plasma instabilities. These general arguments apply both for direct-drive (where the capsule outer wall is directly illuminated with laser light) and indirect-drive (where the laser light or ion beams first converted to x-rays in a radiation cavity, which in turn ablatively implode the capsule) ICF.

We discuss in this paper the hydrodynamic instabilities experimental program being pursued on the Nova laser as part of the ICF effort. In Sec. II, we describe an extensive effort in indirect-drive to investigate hydrodynamic instabilities growing at the ablation front in 2D versus 3D, single-mode versus multimode, and planar geometry versus convergent geometry. We are also investigating imbedded interface instability growth, both in acceleration, and in deceleration. In Sec. III, we review our effort in

direct-drive, by presenting the results from our linear-regime RT experiments, and our laser-imprint experiments for both green and blue laser light. We summarize in Sec. IV.

II. Hydrodynamic Instabilities in Indirect Drive

One of the unique features of laser experiments is the degree of precision possible in selecting the initial conditions of experiments. An excellent example is the recent experimental verification by Marinak *et al.*[Ref] of the differences between two-dimensional (2D) and three-dimensional (3D) Rayleigh-Taylor (RT) induced perturbation growth, as shown in Fig. 1. The experiment was conducted by pre-imposing a precisely formed perturbation on one side of a ~60 μm thick plastic foil doped with bromine, $C_{50}H_{47}Br_3$, or CH(Br). This foil is then placed across an opening on a 3 mm x 1.6 mm gold cylindrical hohlraum. Eight of the ten Nova laser beams are focused into the hohlraum, generating a 1-2 ns pulse of ~200 eV thermal x-rays, which ablatively accelerated the foil at up to ~75 μm/ns^2. The foil is diagnosed in-flight using time resolved face-on radiography. The imposed perturbations at the ablation front grow due to the RT instability. The three perturbations studied in Marinak *et al.* all had the same magnitude wave vector, $k=(k_x^2+k_y^2)^{1/2}$ and the same amplitude, ~2.5 μm, differing only in their shape: 3D square $k_x=k_y$ ($\lambda_x=\lambda_y=71\mu m$), 3D stretched $k_x=3k_y$ ($\lambda_x=53$ μm, $\lambda_y=158$ μm), and a 2D ripple $k=k_x=k_{2D}$ ($\lambda_{2D}=50$ μm). The images shown in Fig. 1a-c correspond to time-resolved, face-on, in-flight radiographs taken of the accelerated planar foils. Dark regions correspond to spikes, and bright regions to bubbles. The growth versus time of the fundamental mode Fourier amplitudes of the perturbations is shown in Fig. 1d. In the linear regime, all three modes grow at the same rate, as expected from linear theory, since they all have the same magnitude wave vector. But in the nonlinear regime, the square $k_x=k_y$ mode grows the largest, the 2D $k=k_x$ ripple grows the least, and

the 3D stretched $k_x=3k_y$ perturbation falls in between. This nonlinear shape effect has been predicted theoretically by several groups,[Ref] but has not been observed experimentally until these laser experiments. As pointed out by Hecht *et al.*,[Ref] this shape effect can be understood qualitatively in terms of a simple buoyancy versus drag argument. In the asymptotic limit of terminal bubble velocity, the buoyancy is exactly balanced by the kinematic drag. At the bubble tip, the ratio of drag/buoyancy is smallest for the square mode, $k_x=k_y$, which consequently has the highest terminal bubble velocity, and therefore grows the fastest.

Our remaining effort in these ablation front RT experiments is to more carefully map out the indirect-drive dispersion curve by developing a longer drive with a period of reasonably constant acceleration. We are also developing 3D multimode targets to test the onset of multimode nonlinear saturation. The drive characterization-dispersion curve work is ongoing, with data analysis in progress.

Rapid material compression leads to the launching of strong shocks, which generate material mixing through the Richtmyer-Meshkov (RM) instability.[Ref] Radiation flow leads to density gradients and to mass ablation, both of which can affect the degree of RT instability growth significantly. This is clearly illustrated in the recent Nova laser experiments of Budil *et al.*,[Ref] who compared RT growth at an ablation front with that at an RT-unstable embedded interface remote from the ablation front, as shown in Fig. 2. In this experiment, the target corresponded to a 35 μm doped plastic ($C_{50}H_{47}Br_3$) ablator, backed by a 15 μm Ti payload, with a 2D sinusoidal ripple at the plastic-metal interface. The experiments were conducted in an otherwise identical fashion to those described in Fig. 1, and the results are shown in Fig. 2. The largest perturbation growth factors (GF) were observed for the shortest perturbation wavelengths, λ=10-20 μm, as shown in Fig. 2d and 2e. For comparison, nearly identical experiments were also done with the perturbations at the ablation front, as shown by the open circle plotting symbols in Fig.

2e. At the ablation front, the growth of perturbations with $\lambda < 50$ μm was strongly inhibited. The combined effects of a density gradient and ablation velocity strongly stabilize growth of short wavelength perturbations at the ablation front, with perturbations of $\lambda \leq 20$ μm essentially not growing at all. Conversely, at the embedded interface, it is precisely the shortest wavelength perturbations that exhibit the largest grow; the maximum observed growth factor in the Budil experiment was at the shortest wavelength imaged, $\lambda = 10$ μm.

This technique has been extended to multimode 2D perturbations. We have done a number of experiments using different combinations of two wavelengths superposed, including pairs of $(\lambda_1, \lambda_2) =$ (100, 20 μm), (10, 15 μm), as shown in Fig. 2f, and (4, 5 μm), as shown in Fig. 2g. The latter pattern is interesting because the 4 and 5 μm wavelengths are below the experimental resolution of ~10 μm. But these wavelengths correspond to the fifth and fourth harmonics of the $\lambda_{fund} = 20$ μm. Once the perturbation development enters the nonlinear regime, second order perturbation theory predicts coupling to occur via $\eta_{i\pm j} = -+1/2\ (k_i \pm k_j)\eta_i\eta_j$ for the amplitude of the coupled mode. The k5-k4 mode corresponds to $\lambda_{fund} = 20$ μm, which is easily within the experimental resolution. We show this image in Fig. 2g as the Fourier distribution at t=5 ns. The 20 μm fundamental clearly stands out well above the experimental noise. Hence, by judicious choice of two superposed patterns, and using second order perturbation theory, we have effectively extended the resolution of our gated x-ray pinhole camera down to 4 μm. The goal of this experimental effort is to measure a multimode pattern, investigating the onset of multimode nonlinear saturation and inverse cascade (i.e., bubble merger in physical space). We show one 20-mode initial perturbation in Fig. 2h, where the modes corresponded to the first 20 harmonics of λ_{fund}=200 μm, and the amplitudes were chosen at random. The Fourier distribution at t = 5 ns is shown in Fig. 2i. In this shot, the overall growth factors were modest, and a strong inverse cascade was

not yet observed. By going to a band of modes $\lambda_n=\lambda_1/n$, n=10-20, for λ_1=100 μm, we hope that a significant inverse cascade will be observable, and experiments are planned to look for this.

Precise experiments such as the planar ablation-front experiments shown in Fig. 1 can also be carried out in convergent geometries. This is illustrated in Fig. 3 with preliminary results from two new experiments in convergent geometry. The first, by Glendinning *et al.*[Ref] measures the growth of a 3D $k_x=k_y$ square mode perturbation (here, $\lambda_x=\lambda_y$=100 μm), but this time in spherically converging geometry. Here, the perturbation was imposed on the outer surface of a ~500 μm diameter hemisphere of germanium-doped plastic ($C_{50}H_{48.8}Ge_{1.2}$), which was mounted on the wall of a hohlraum, facing inwards. As the hemisphere is ablatively accelerated, the perturbations grow due to ablation front RT instability at the same time that the hemisphere converges. This is illustrated in Fig. 3a-d with a sequence of face-on radiographs. Figure 3e shows $\lambda_x=\lambda_y$ as a function of time, decreasing from 100 μm to 60 μm, for a total convergence, R_o/R, of just under 2. Figure 3f shows the growth of the fundamental and second harmonics of the perturbation in terms of δ(optical depth), versus time. The perturbation enters the nonlinear regime at ~2 ns, as is evidenced by appearance of the second harmonic. Notice, however, that the growth factor (GF) is only 2.0-2.5. On a planar foil, this amount of growth for an η_o=2.5 μm, $\lambda_x=\lambda_y$=100 μm perturbation would still be in the linear regime, since $\eta/\lambda < 10\%$. The early entry into the nonlinear regime observed here is due to convergence, that is, the wavelength decreasing from 100 μm to 60 μm. For the same overall growth of η, now η/λ is larger because λ is smaller, and the RT evolution has consequently entered the nonlinear regime.

We have also done radiography of capsules imploding at the center of the hohlraum. These experiments were designed initially to measure the capsule in-flight aspect ratio (R_o/R) and density profiles, to compare capsule performance with and

without a dopant in the ablator serving as a preheat shield.[Ref] Considerable effort went in to developing the means to lower the background level in the data. We have lowered the experimental background by going to thicker substrates for the pinholes (3 mil Ta instead of 2 mil), attaching a thick colimater with 70 μm pinhole apertures, and by thickening the side of the hohlraum facing the diagnostic. Our latest results show that the data are now very clean, and allow analysis to determine in-flight aspect ratio. Experiments are now underway to compare in-flight aspect ratio for doped CH(Ge) versus undoped CH capsules. A more interesting application of this technique is to image a perturbed capsule, as shown in Fig. 3g-i. The perturbation pattern imposed was a set of three groves. The perturbation growth is clearly visible, with dark bands corresponding to spikes and light bands to bubbles, and compares very well with simulations, as shown in Fig. 3j.

III. Hydrodynamic Instabilities in Direct Drive

We have also been pursuing RT experiments in direct drive. In Fig. 4a we show the results of a RT experiment where direct illumination of green laser light (2ω, λ_L=0.528 μm) onto a 20 μm thick CH_2 foils (ρ=0.95 g/cm^3), giving a 2 ns ~constant acceleration of ~50 μm/ns^2. The data shown in Fig. 4a corresponds to a sinusoidal ripple of λ=70 μm, η_o=0.5 μm imposed on the illumination side of the foil. Since the amplitude was intentionally chosen to be small, the RT evolution remained in the linear regime, which for constant acceleration, leads to the observed exponential growth, $\eta(t)=\eta_o e^{\gamma t}$, where η is perturbation amplitude, and γ is the RT growth rate. The results of a wavelength scaling series of these experiments, spanning wavelengths of 20-70 μm is shown in Fig. 4b in terms of measured growth rate γ_{RT} vs wavelength. Even though there is some scatter in the data, it appears that over the range measured, the growth rate γ_{RT} is approximately flat as a function of perturbation wavelength, λ. The results of the LASNEX simulations are shown in both Figs. 4a and 4b. LASNEX systematically over

predicts the growth rate at the short wavelengths. Our simulations have been using flux limited diffusion for the heat transport. If instead we do a 1D analysis with Fokker-Planck transport, then invert to predict what we would have observed for growth rate, using a Takabe-like dispersion curve, we get the lower dotted curve in Fig. 4b. The data appear to lie in-between, suggesting that refinements in how heat transport is modeled potentially could resolve this discrepancy with observation.[Ref]

We have also done a series of laser imprinting studies on Nova. We show recent results in Fig. 4c and 4d . In this investigation, we compared imprint levels for blue (λ_L=0.351 μm) versus green (λ_L=0.528 μm) at otherwise identical conditions. Here we used a static RPP speckle pattern to generate a static imprinting modulation at the target. Raw images are shown in Fig. 4c and the analyzed power spectra are shown in Fig. 4d . It is evident both from the raw data and the Fourier analysis that the blue light imprints laser nonuniformities onto the target more strongly that the green light. Correcting for systematic differences between the shots, we show the imprint efficiency for both experiments (blue versus green) in Fig. 4d . For modes $n \leq 10$, the blue drive imprints target perturbations ~50% more efficiently than the green drive. Our conclusion here is that the green laser imprints less due to the development of a standoff layer between the critical surface and the ablation front. This standoff layer smoothes out some of the laser nonuniformities, before they reach the ablation front, and imprint onto the target. Results of a simple "cloudy day" model, which quantifies this simple argument, are also shown in the figure by the two dashed curves, and is consistent with our conclusion.

IV. Summary

In summary, we are investigating hydrodynamic instabilities both in planar and in spherical geometry, and in indirect- and direct-drive. In indirect drive, specific issues in the instability evolution that we are examining are RT growth of 2D versus 3D single-

mode perturbations, the effect of drive pulse shape, perturbation location at the ablation front versus at an embedded interface, and multimode perturbation growth and nonlinear saturation. The effects of convergence on RT growth are being investigated both with hemispherical implosions of packages mounted on the hohlraum wall and with spherical implosions of capsules at the center of the hohlraum. Single-mode perturbations are pre-imposed at the ablation front of these capsules as a seed for the RT growth. In our direct drive experiments, we are investigating the effect of laser imprinting and subsequent RT growth on planar foils, both at λ_{Laser}=1/3 μm and 1/2 μm. An overview is given describing recent progress in each of these areas.

Acknowledgements

*Work performed under the auspices of the U.S. Department of Energy by the Lawrence Livermore National Laboratory under contract number W-7405-ENG-48.

References

[1]J.D. Kilkenny *et al.*, Phys. Plasmas **1**, 1379 (1994).

[2]B.A. Hammel *et al.*, Phys. Fluids B **5**, 2259 (1993); Phys. Plasmas **1**, 1662 (1994).

[3]M.M. Marinak *et al.*, Phys. Rev. Lett. **75**, 3677 (1995); Phys. of Plasmas, in press (July, 1996).

[4]S.V. Weber *et al.*, Phys. Plasmas **1**, 3652 (1994).

[5]K.S. Budil *et al.*, submitted, Phys. Rev. Lett. (1996); Bull. Am. Phys. Soc. **40**, 1749 (1995).

[6]B.A. Remington *et al.*, Phys. Rev. Lett. **73**. 545 (1994); Phys. Plasmas **2**, 241 (1995).

[7]D.H. Kalantar *et al.*, Bull. Am. Phys. Soc. **40**, 1856 (1995).

[8]J. Kane *et al.*, Bull. Am. Phys. Soc. **40**, 1841 (1995); M. Wood-Vasey *et al.*, Bull. Am. Phys. Soc. **40**, 1841 (1995).

[9]E. Müller, B. Fryxell, and D. Arnett, Astron. Astrophys. **251**, 505 (1991).

[10]S.G. Glendinning *et al.*, Phys. Rev. Lett. **69**, 1201 (1992); submitted, Phys. Rev. Lett. (1996).

[11]D.H. Kalantar *et al.*, in press, Phys. Rev. Lett. (April, 1996); Bull. Am. Phys. Soc. **40**, 1749 (1995).

References

Figure 1. Results from indirect-drive experiments examining single-mode, Rayleigh-Taylor growth at an ablation front in 2D versus 3D.

Figure 2. Results from indirect-drive experiments examining 2D Rayleigh-Taylor growth at an embedded interface, for single modes, two superposed modes, and a spectrum of 20 modes.

Figure 3. Results from indirect-drive experiments examining "single-mode" Rayleigh-Taylor growth at an ablation front in converging geometry, both on imploding hemispheres, and on full capsule implosions.

Figure 4. Results from direct-drive experiments examining (a,b) linear regime single-mode, Rayleigh-Taylor growth at an ablation front in 2D, and (c,d) imprinting due to laser nonuniformities, comparing green with blue light.

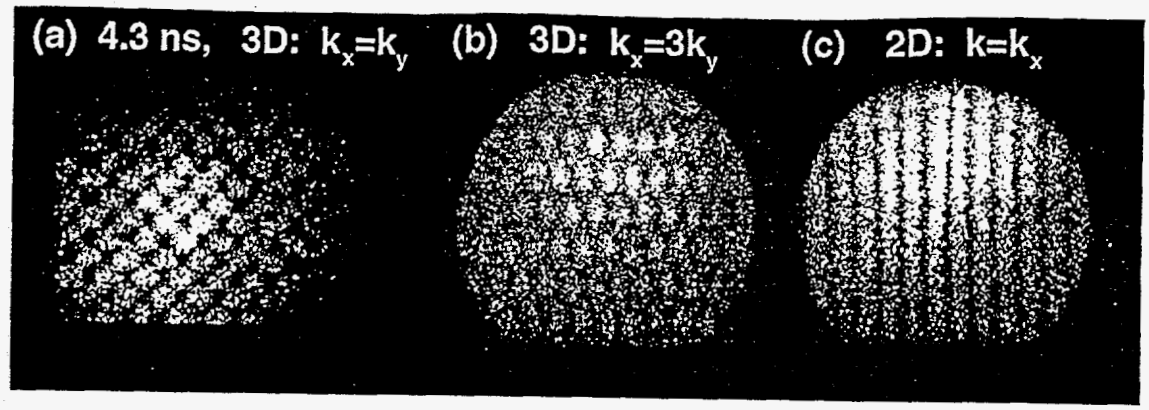
(a) 4.3 ns, 3D: $k_x=k_y$
(b) 3D: $k_x=3k_y$
(c) 2D: $k=k_x$

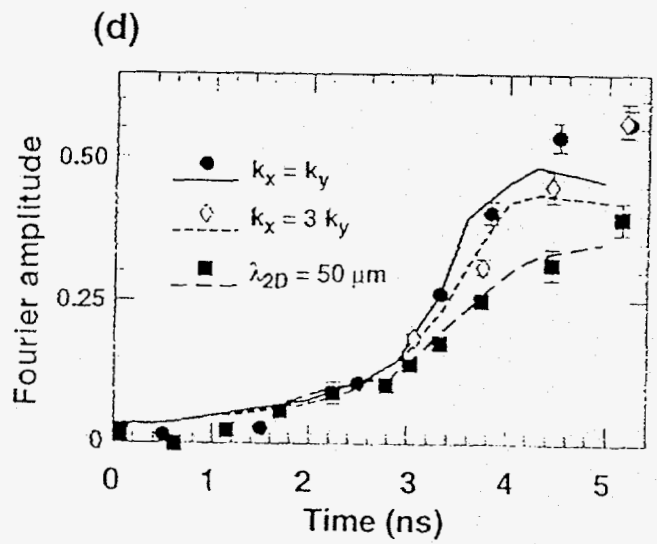
(d)
Fourier amplitude
0.50
0.25
0
$k_x = k_y$
$k_x = 3\ k_y$
$\lambda_{2D} = 50\ \mu m$
0
1
2
3
4
5
Time (ns)

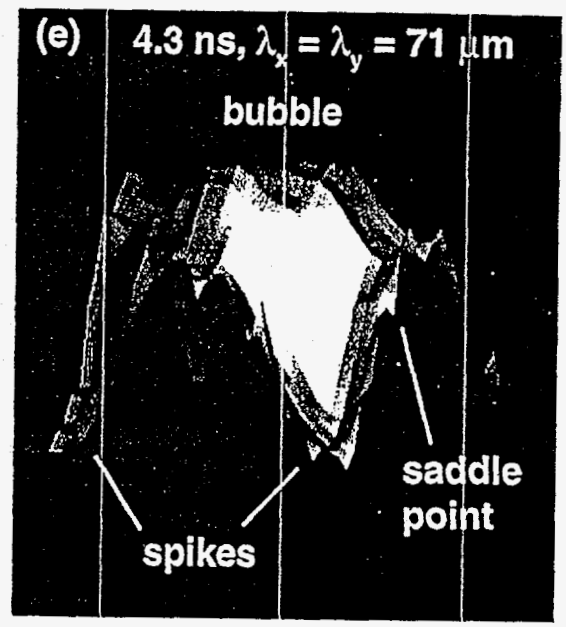
(e)
4.3 ns, $\lambda_x = \lambda_y = 71\ \mu m$
bubble
saddle point
spikes

Fig 1

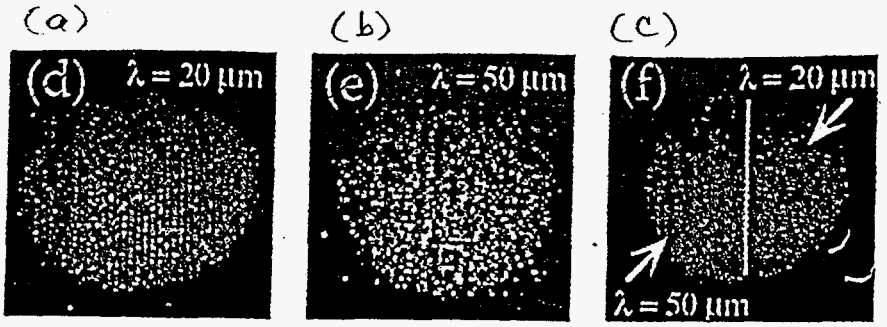
(a)
(b)
(c)
(d) λ = 20 μm
(e) λ = 50 μm
(f) λ = 20 μm
λ = 50 μm

4.8 nsec

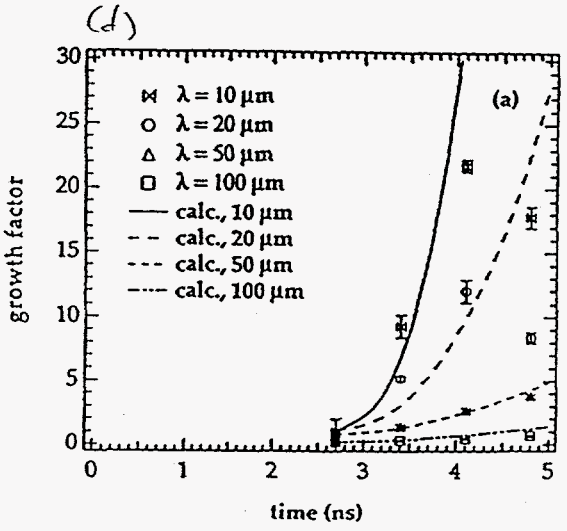
(d)
λ = 10 μm
λ = 20 μm
λ = 50 μm
λ = 100 μm
calc., 10 μm
calc., 20 μm
calc., 50 μm
calc., 100 μm
(a)
growth factor
time (ns)

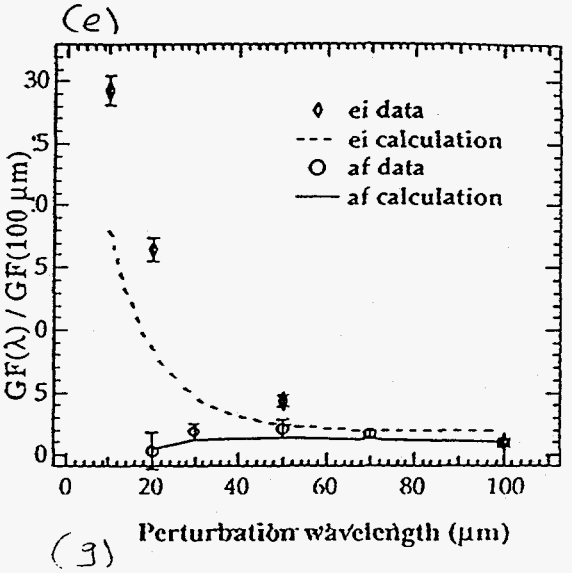
(e)
ei data
ei calculation
af data
af calculation
GF(λ) / GF(100 μm)
Perturbation wavelength (μm)

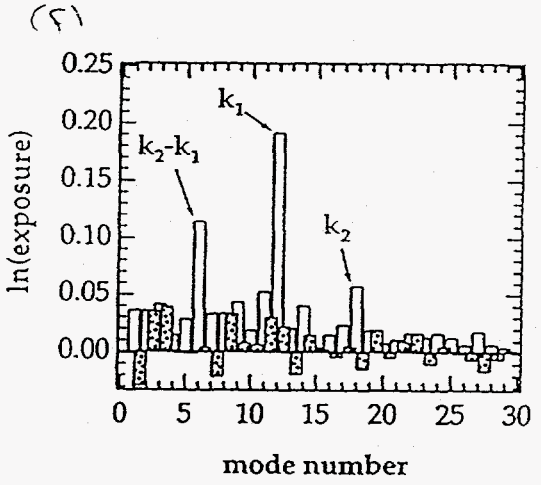
(f)
k1
k2-k1
k2
ln(exposure)
mode number

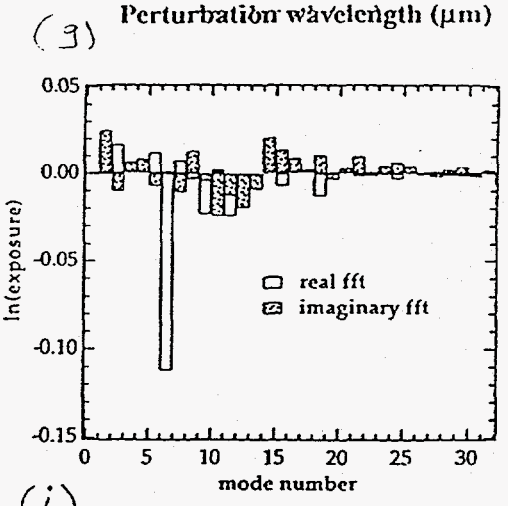
(g)
real fft
imaginary fft
ln(exposure)
mode number

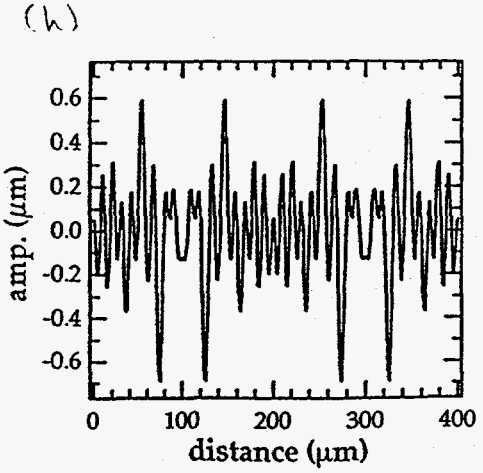
(h)
amp. (μm)
distance (μm)

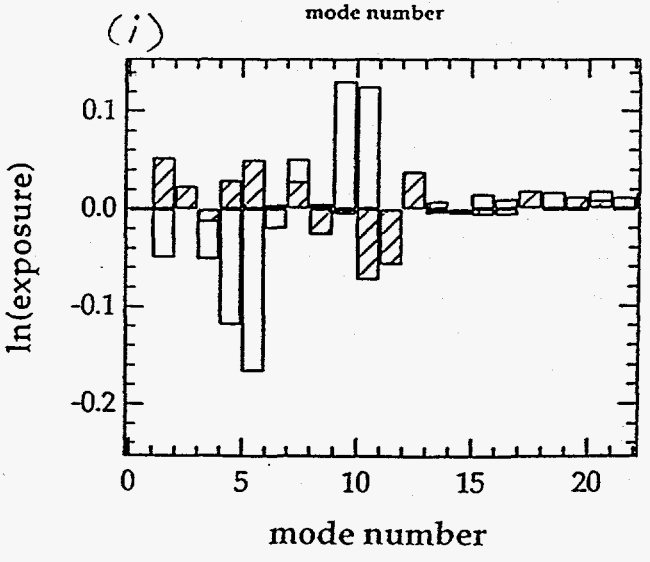
(i)
ln(exposure)
mode number

Fig 2

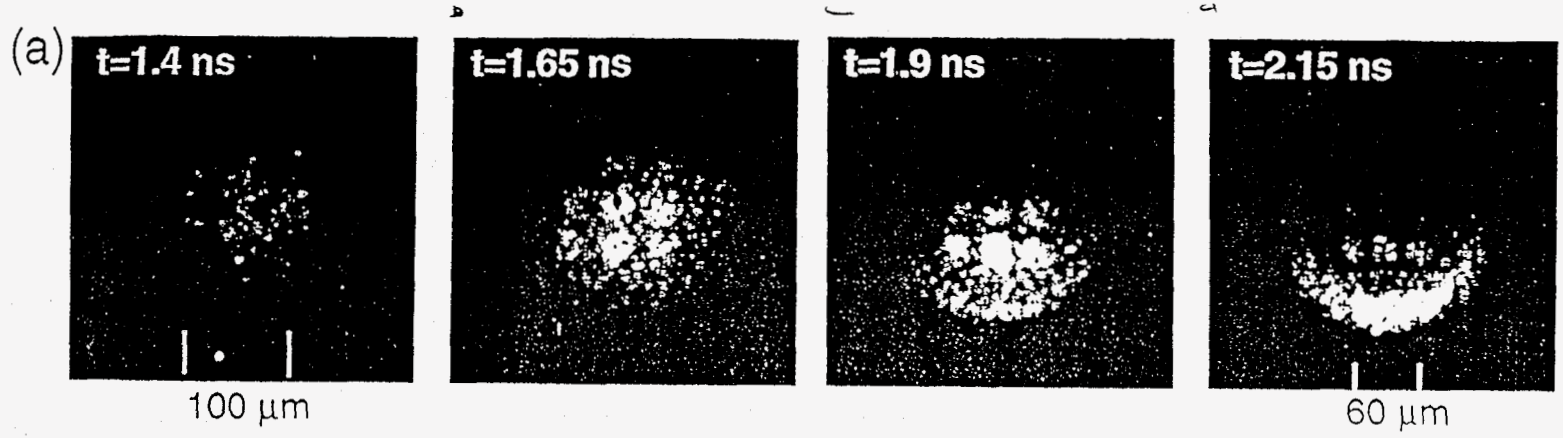
(a)
t=1.4 ns
t=1.65 ns
t=1.9 ns
t=2.15 ns
100 μm
60 μm

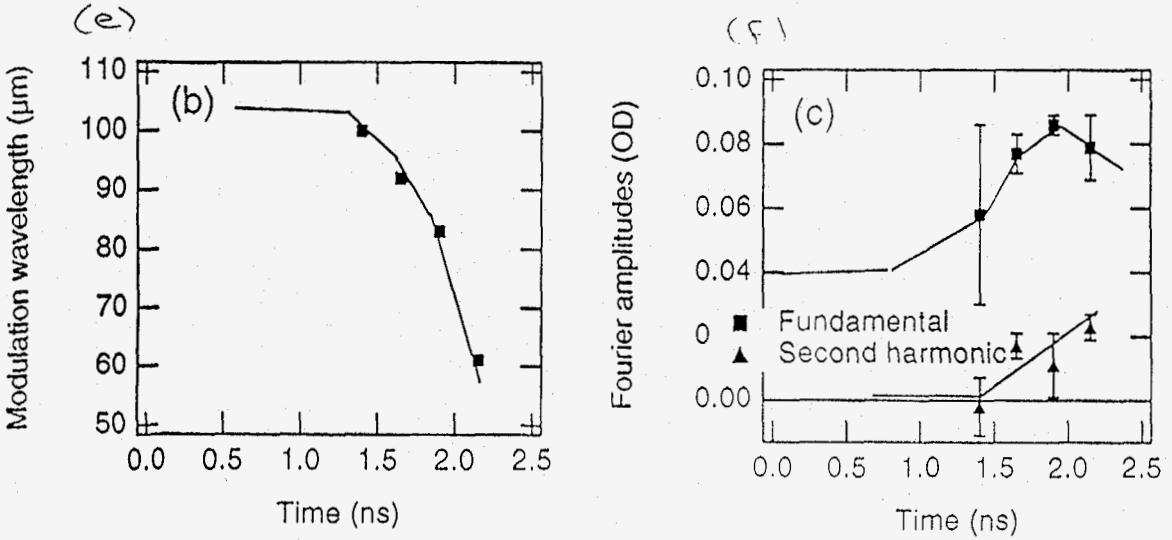
(e)
(b)
Modulation wavelength (μm)
110
100
90
80
70
60
50
0.0 0.5 1.0 1.5 2.0 2.5
Time (ns)
(f)
(c)
Fourier amplitudes (OD)
0.10
0.08
0.06
0.04
0
0.00
Fundamental
Second harmonic
0.0 0.5 1.0 1.5 2.0 2.5
Time (ns)

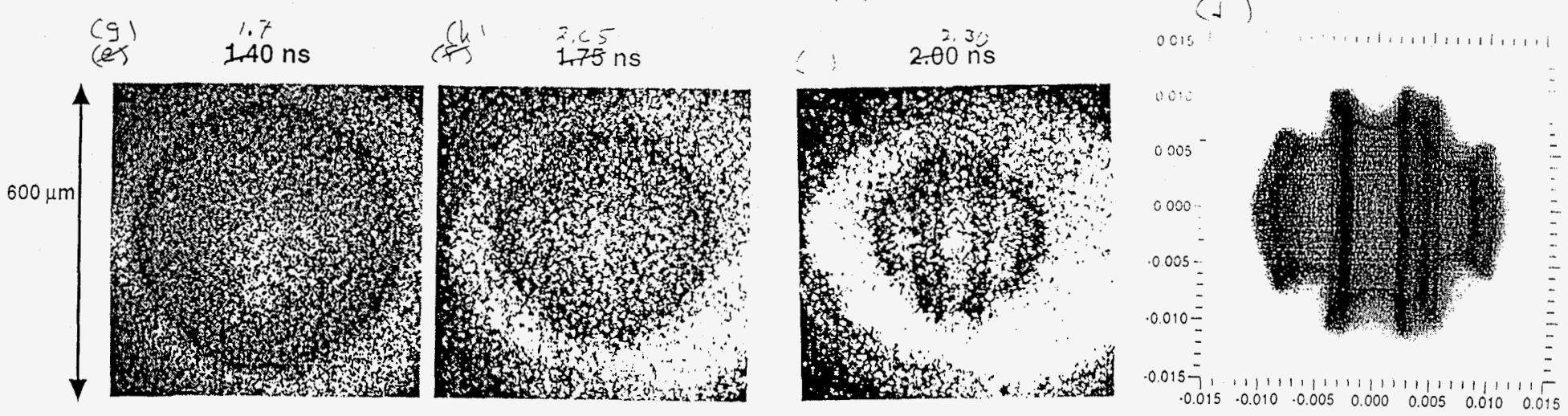
(g)
(e)
1.7
1.40 ns
(h)
(f)
2.05
1.75 ns
(i)
2.30
2.00 ns
600 μm
(j)
0.015
0.010
0.005
0.000
-0.005
-0.010
-0.015
-0.015 -0.010 -0.005 0.000 0.005 0.010 0.015

Fig. 3

(a)

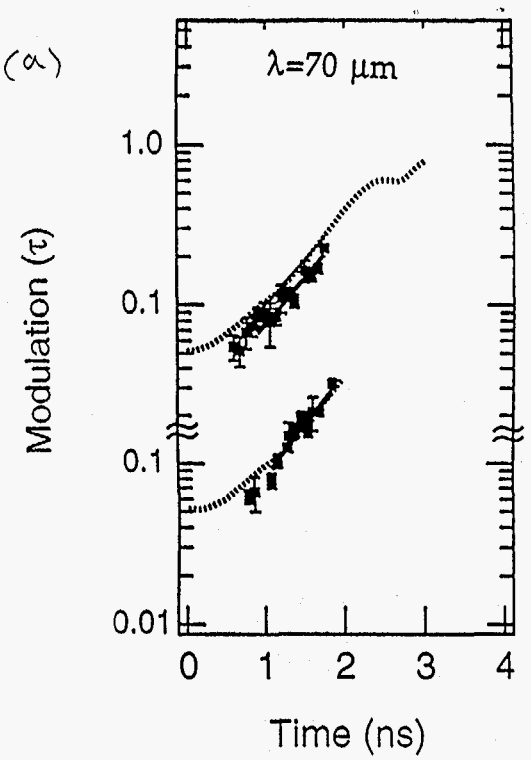
λ=70 μm
1.0
0.1
0.1
0.01
Modulation (τ)
0
1
2
3
4
Time (ns)

(b)

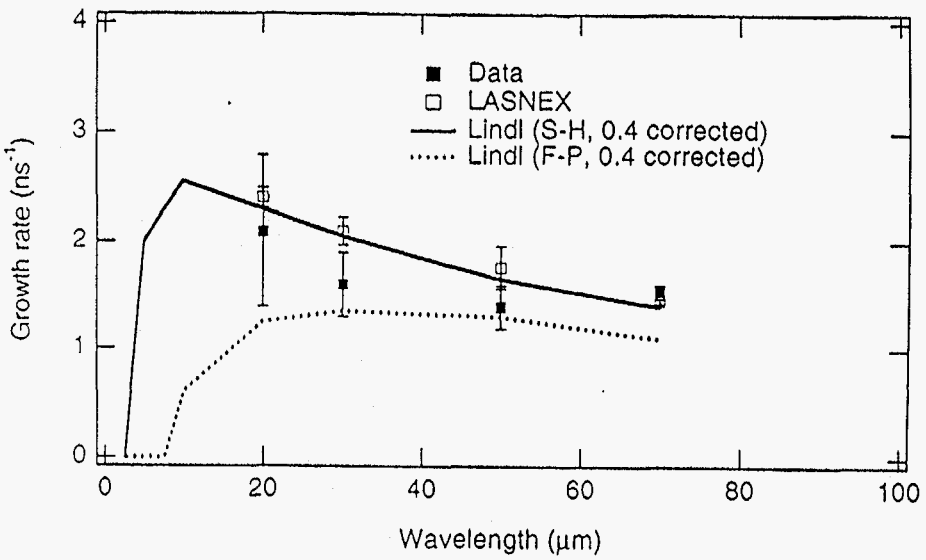
Data
LASNEX
Lindl (S-H, 0.4 corrected)
Lindl (F-P, 0.4 corrected)
Growth rate (ns^{-1})
0
1
2
3
4
0
20
40
60
80
100
Wavelength (μm)

(c)

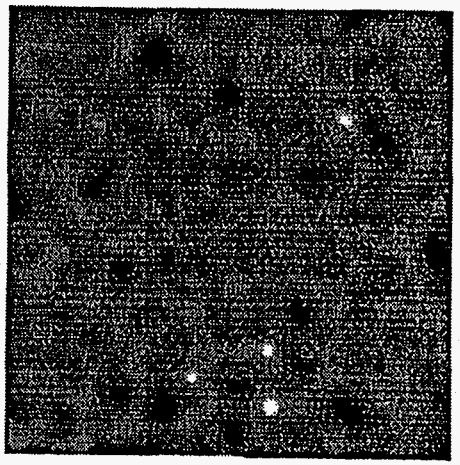

(d)

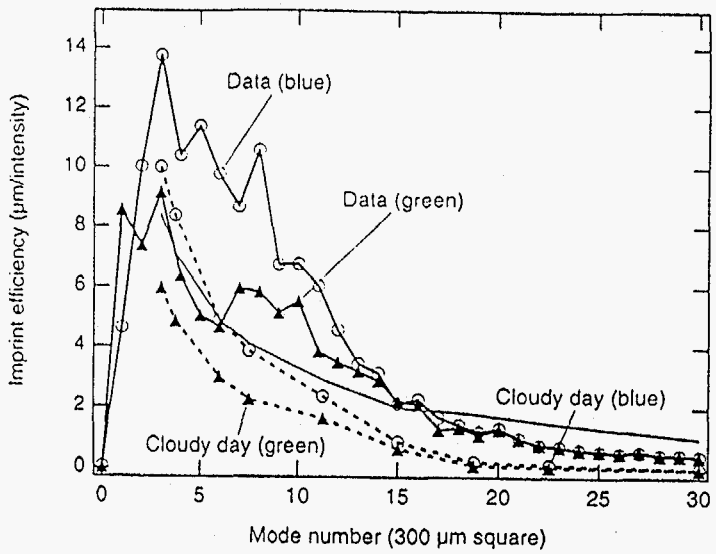
Data (blue)
Data (green)
Cloudy day (blue)
Cloudy day (green)
Imprint efficiency (μm/intensity)
0
2
4
6
8
10
12
14
0
5
10
15
20
25
30
Mode number (300 μm square)

Fig 14